

1  
2  
3  
4 **Static Mode Microfluidic Cantilevers for Detection of Waterborne Pathogens**

5  
6 Helen Bridle<sup>1,2</sup>, Wenxing Wang<sup>1</sup>, Despoina Gavriilidou<sup>2</sup>, Farid Amalou<sup>1</sup>, Duncan P.  
7 Hand<sup>3</sup>, Wenmiao Shu<sup>1</sup>  
8

9 1) Institute of Biological Chemistry, Biophysics and Bioengineering, School of  
10 Engineering and Physical Sciences, Heriot-Watt University, EH14 4AS

11 2) School of Engineering, University of Edinburgh, King's Buildings, EH9 3JJ  
12 (when the work was done); now Imperial College London

13 3) Institute of Photonics and Quantum Sciences, School of Engineering and  
14 Physical Sciences, Heriot-Watt University, EH14 4AS

15 Corresponding author: [h.l.bridle@hw.ac.uk](mailto:h.l.bridle@hw.ac.uk); 0131 451 3355  
16

17 **ABSTRACT:** This paper reports on the first demonstration of polymeric microfluidic  
18 cantilever sensors. Microcantilever sensors, magnetic beads, and microfluidic  
19 technology has been combined to create a polymer based biosensor. Using cheap  
20 materials like polyimide, a simple fabrication method has been developed to produce  
21 cantilevers with an embedded microfluidic channel. The advantage of this approach is  
22 that the addition of a microfluidic channel enables the analysis of smaller volumes  
23 and increases the capture efficiency in applications detecting rare analytes. As a proof  
24 of principle the system has been applied for the detection of the waterborne protozoan  
25 parasite *Cryptosporidium*, achieving sensitivity comparable to QCM, whereas a  
26 previous set-up without the microfluidic channel was unable to detect the parasite.  
27

28 **Keywords:** microfluidics, cantilever, *Cryptosporidium*, detection  
29  
30  
31  
32  
33  
34  
35

36

## 37 **Introduction**

38

39 Cantilever biosensors have demonstrated impressive sensitivity for the  
40 detection of nuclei acids, proteins and cells [1-4]. However, in solution, when  
41 operated in the resonance mode, viscous damping severely degrades the resolution  
42 [5]. Alternatively, cantilevers can be operated in static mode, with surface stress  
43 determining the degree of cantilever bending. While this eliminates the problem of  
44 viscous damping for measurements in liquid, the challenge then becomes effective  
45 delivery of the sample to the cantilever surface. This challenge is especially important  
46 in applications where relatively large analyte sample volumes are necessary, e.g.  
47 environmental monitoring [6]. In order to address this, immobilisation strategies can  
48 be optimised to attempt to maximise capture efficiency of the sensor or external  
49 forces can be utilised to enhance delivery [7].

50

51 Previously, cantilevers have been embedded within microfluidic systems [8,  
52 9]; and more recently, smaller-scale microfluidics which fits onto the cantilever  
53 surface itself is demonstrated. For example, the Manalis group have developed  
54 microfluidics upon cantilevers, manufactured from silicon and employed in the  
55 resonance mode. This highly successful strategy has lead to the weighing of single  
56 cells in fluid [5]. Very few other microfluidic cantilever systems have been reported  
57 [10]. However, the materials and fabrication approaches are expensive. Additionally,  
58 while the latter work provides an interesting method of weighing individual  
59 microorganisms, specificity in pathogen detection is not offered.

60

61 *Cryptosporidium* is a protozoan pathogen, which is highly problematic for the water  
62 industry due to a low infectious dose [11] and high degree of robustness which  
63 enables long survival times in water along with resistance to standard disinfection by  
64 chlorination [12]. Several biosensor technologies have been applied to the detection of  
65 *Cryptosporidium* as reported in a recent review article [13]. Both quartz crystal  
66 microbalance (QCM) [14] and piezoelectric macrocantilever (PEMC) [15] approaches  
67 utilised relatively large flow cells and delivery of the sample to the sensor surface was  
68 not characterised.

69

70 Here we present the low-cost manufacture of polymeric microfluidic cantilevers and  
71 demonstrate the effectiveness of this set-up in improving transport to the sensor in  
72 both the detection of pathogens and DNA. The approach reported here has the  
73 advantage of ensuring effective sample delivery to the surface of the sensor, enabling  
74 high capture efficiency, which is useful in the situation of detecting rare pathogens.  
75 Miniaturisation of sample delivery in this way limits the throughput of devices,  
76 although there is potential to negate this problem through parallelisation or effective  
77 sample pre-processing. Previous unpublished work by the authors using  
78 microcantilevers without microfluidic channels presented low sensitivity to  
79 *Cryptosporidium* oocysts whereas use of the microfluidic channel has enabled a  
80 detection limit of  $1 \times 10^5$  oocysts/mL. However, the main advantage of the system  
81 presented here over previous microfluidic cantilever set-ups is that since the device is  
82 made entirely of polyimide it is both cheaper and easier to manufacture.

83  
84

## 85 **2. Materials and Methods**

86

### 87 **2.1 Cantilever manufacture**

88 The sensor was precision fabricated using a photolithography method. Firstly,  
89 a sheet of polyimide (7.6 micron thick, 3 inch x 50 inch, VHGLABS Kapton®  
90 (Polyimide)) was sputter-coated with an adhesive layer of chrome (5 nm) followed by  
91 a layer of gold (20 nm) using gold evaporation system (BOC Edwards Auto 500).  
92 Secondly, this gold-coated polyimide was attached to a sheet of 20  $\mu\text{m}$  thick positive  
93 photoresist (photopolymer dry film resist, ORDYL), and the two sheets were bonded  
94 together using pressure applied at 95°C. Thirdly, a mask (fabricated by  
95 microlithography) was employed to control the UV exposure (exposure time of 30  
96 seconds) creating patterns of microchannels. Fourthly, the UV exposed sheet was  
97 developed (Developer conc. for 4615 dry film Mega Electronics Ltd) for 20 seconds  
98 removing the positive photoresist in the exposed areas. These areas define the  
99 microfluidic channels. Fifthly, the microchannels were sealed using 25  $\mu\text{m}$  polyimide  
100 tape as a top layer. This process is summarised in Figure 1A. Finally, a short pulsed  
101 (65 ns) laser of wavelength 532 nm was used to cut the structures into individual  
102 microcantilever microfluidic chips, with cantilever dimensions of 1.5 mm in length  
103 and 300  $\mu\text{m}$  in width. Each cantilever contained one U shaped microfluidic channel

104 with channel sizes of 60  $\mu\text{m}$  in width, 20  $\mu\text{m}$  in height and total of 3 mm in length  
105 (Figure 1B).

106

## 107 2.2 Cantilever Set-Up and Operation

108

109 The cantilever set-up developed in this paper includes a rotary valve, microcantilever  
110 chip with a microchannel fabricated on top that is connected with tubing to a gravity  
111 fed pumping system (1) via the rotary valve (2), laser diode (7), position-sensitive  
112 detector (PSD) (8), a magnet and microscope with a digital CCD camera (9) (Figure  
113 1C; numbers relate to the labels in Figure 1C). The cantilever system is set up on an  
114 optical table (4) (Newport Laminar Flow isolator) to reduce vibrations. The system is  
115 mounted in a non-transparent box (3) made of PMMA (5mm thickness), with thermal  
116 insulated materials (10mm thickness), which reduces the external disturbance from air  
117 flow, background light, and temperature variations in the lab [ $\pm 0.5$  degree]. The  
118 rotary valve switch device is computer-controlled via RS-232 and is used to switch  
119 between the flow different liquids into the microchannel on the cantilever surface.  
120 With the use of the rotary valve, in addition to gravity pumping of the liquid (1 mL/h),  
121 spikes in the results curve can be significantly reduced. The optical resolution of the  
122 microscope is 5  $\mu\text{m}$ , which is used to confirm that the laser beam is on the tip of the  
123 cantilever. The laser beam reflected by the cantilever is aligned on to a position-  
124 sensitive detector (PSD) and an amplifier is used to amplify the current signal from  
125 the PSD and convert into voltage signals. A National Instrument data acquisition card  
126 is then used to record data in LabView.

127

## 128 2.3 Detection of *Cryptosporidium*

129

130 Reagents: Viable *C. parvum* oocysts were purchased from Creative Science  
131 Company, Moredun Research Institute. Magnetic beads and goat polyclonal antibody  
132 immunoglobulin G (IgG) specific to *C. parvum* were purchased from Waterborne Inc.  
133 Phosphate-buffered saline (PBS) was obtained from Sigma-Aldrich.

134

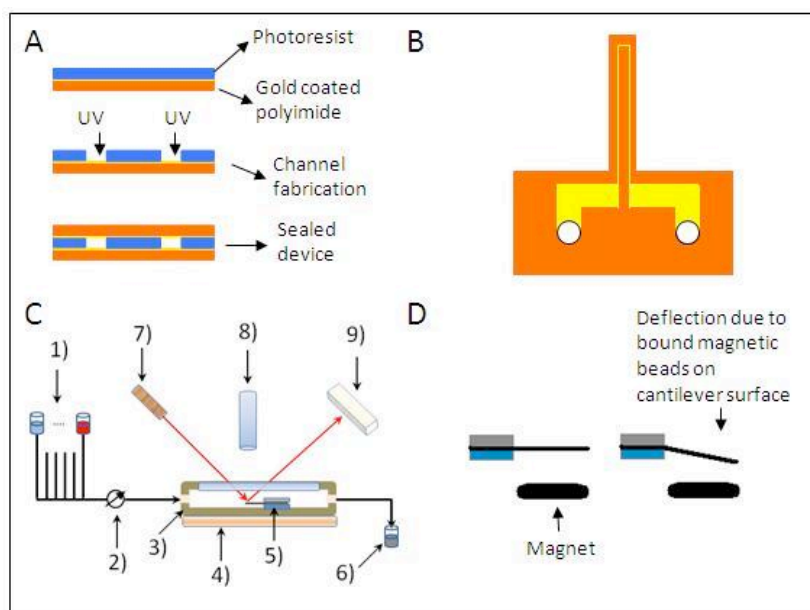
135 Functionalization of cantilever microfluidic biosensor with protein G, antibody IgG  
136 and immobilization with *C. parvum* solution: The sensor was functionalized with

137 protein G solution (20 mg/mL) for 2 hours, IgG solution (20  $\mu\text{g/mL}$ ) for another 2  
138 hours [16] and finally exposed to *C. parvum* solution (between  $1 \times 10^5$  oocysts/mL and  
139  $1 \times 10^7$  oocysts/mL in DI water) for 10 mins causing the oocysts' immobilization on the  
140 surface of the sensor. After each step was complete, the sensor was rinsed with PBS  
141 solution (10mM, pH 7,4). After immobilization of oocysts, the biosensor was left to  
142 stabilize and afterwards it was incubated with magnetic beads solution (Crypto-Grab,  
143 Waterborne Inc, 2.5 mg/mL) for 20 minutes. Finally the sensor was rinsed with PBS  
144 solution. Every rinsing was performed in order to remove the unbound reagents. The  
145 protocol was performed in room temperature. The flow rate for all steps was 1 mL/hr.  
146  
147

### 148 3. Results and Discussion

#### 149 3.1 Cantilever manufacture

150  
151  
152 Microfluidic channels embedded in silicon cantilevers have previously been  
153 manufactured using dry etching. In order to utilise low-cost polyimide materials an  
154 alternative fabrication method was required for the production of microfluidic  
155 channels. A method using simple lithographic techniques was employed, as described  
156 in detail in the materials and methods, and illustrated in Figure 1B.



157

158

159 Figure 1. Scheme of integrated microfluidic microcantilever sensor. A) Schematic of the fabrication  
160 process. B) Layout of the microfluidic channel on the cantilever. C) Cantilever set-up. D) Operation of

161 the cantilever sensor with the magnet.

162

163

### 164 3.2 Cantilever Characterisation

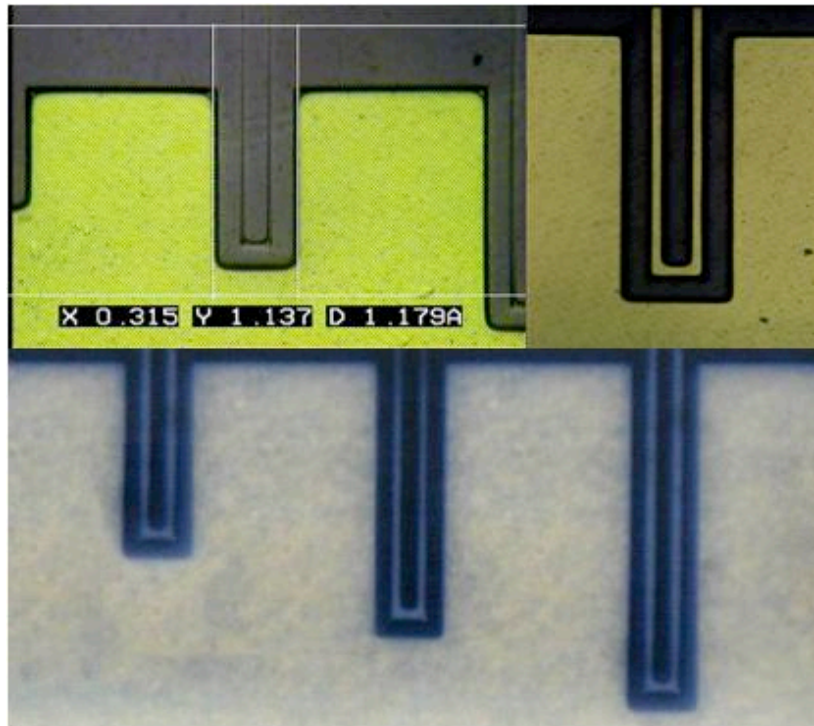
165

166 Following production of the cantilevers, the system was characterised using  
167 optical microscopy. Figure 2A shows an optical microscope image of polyimide  
168 fabricated cantilevers with embedded microchannels. The width of the cantilever was  
169 designed to be 300  $\mu\text{m}$  and the channel is 60  $\mu\text{m}$  wide. Images from several  
170 cantilevers were taken, and an average of X measurements revealed the channel width  
171 was  $X \mu\text{m} \pm 3 \mu\text{m}$ , illustrating that the variability in fabrication was small and that this  
172 is therefore a reproducible method. The images illustrate that cantilevers of different  
173 lengths can be manufactured using this protocol, though for all subsequent  
174 experiments cantilevers of length 1.5 mm were employed.

175

176 In the cantilever set-up illustrated in Figure 1C cantilever performance was  
177 tested. Flow through the microfluidic channel had no influence upon deflection with  
178 the cantilever remaining stable. Various flow rates were trialled and an upper limit  
179 of 1mL/hr was determined. This was limited primarily by the choice to operate using  
180 gravity driven flow. While the bonding technique could tolerate higher pressures, and  
181 therefore flow rates, pumping of fluids through the channel was observed to result in  
182 spikes in the cantilever read-out.

183

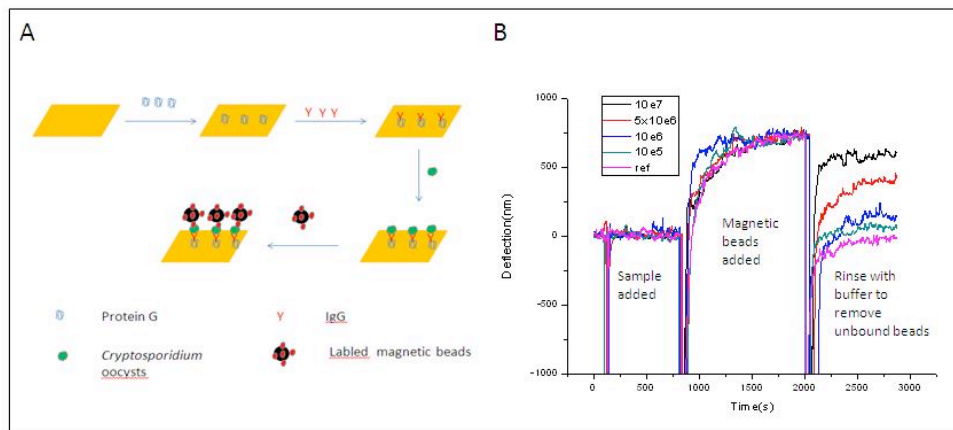


184

185 Figure 2. Cantilever characterisation. Optical microscope images of fabricated microchannels on  
186 microcantilevers.

187

188 The final performance characterisation involved system calibration with  
189 magnetic beads (Figures 1D and 2B). Figure 3A illustrates the schematic of detection  
190 employed for the waterborne parasite under investigation. Detection of whole cells is  
191 challenging in mass-sensitive systems as coupling of the binding event to the system  
192 deflection is critical and this is often weak for larger analytes like cells. Additionally,  
193 factors such as surface stress also contribute to the observed signal. Therefore, the use  
194 of magnetic beads was selected to amplify the signal. Figure 1D illustrates the  
195 operation and set-up with this detection principle with a magnet located beneath the  
196 cantilever holder. To determine that the magnet strength and magnetic bead  
197 concentration were appropriate a series of experiments flowing different  
198 concentrations of magnetic beads through the system were performed. As seen in  
199 Figure 2B, quantitative results were obtained with a series of dilutions indicating that  
200 the cantilever read-out was proportional to the magnetic bead concentration within the  
201 channel, thus confirming this approach was suitable for quantitative pathogen  
202 detection.



204

205 Figure 3. Cantilever detection of waterborne pathogens. A) Schematic illustrating the functionalisation  
 206 of the cantilever to detect *Cryptosporidium* oocysts and the addition of magnetic beads which enables  
 207 enhancement of the detection signal. B) Detection of oocysts at a range of different concentrations  
 208 ranging from a control sample of zero to a set of concentrations from  $1 \times 10^5$  to  $1 \times 10^7$  oocysts. Initially  
 209 the oocysts solution is passed through the cantilever microchannel and although binding takes place  
 210 this is insufficient to trigger cantilever bending. After the introduction of the sample a brief rinsing step  
 211 with PBS is applied. Subsequently, magnetic beads are passed through the channel (at this stage where  
 212 the beads are incubated in the channel little difference is observed between different oocyst  
 213 concentrations) and finally the channel is rinsed with buffer removing any unbound beads. In the final  
 214 stage of the results curve, the measurement of deflection indicates the amount of bound microbeads,  
 215 and therefore also the concentration of oocysts within the cantilever channel, and it is clear that the  
 216 biosensor can distinguish between different concentrations of pathogen.

217

### 218 3.3. Pathogen Detection

219

220 The microfluidic cantilever system was applied to the detection of the  
 221 waterborne protozoan pathogen, *Cryptosporidium*. Detection of this pathogen is  
 222 challenging since it is often present at low concentrations. However, since ingestion  
 223 of only a few oocysts is sufficient to cause disease it is important to maximise capture  
 224 efficiency of oocysts within any biosensor system.

225

226 Our initial work (unpublished) exploring the potential of cantilever sensors to  
 227 detect this pathogen were unpromising with the parasite going undetected even at high  
 228 concentrations. The most likely explanation for this was the sample size and time  
 229 required for delivery of the pathogen to the surface. Since, an identical set-up was  
 employed during cantilever functionalisation, limitations in delivery of one of the

230 immobilisation reagents and/or the antibody to the surface might also have  
231 contributed to the poor detection.

232

233 The time allowed for oocyst exposure to the surface was 10 mins. In the set-up  
234 without a flow system using 1mL of solution the time was insufficient to result in a  
235 high capture efficiency on the cantilever surface. The time taken,  $t$ , for a particle to  
236 diffuse a distance,  $d$ , is given by:

$$237 \quad d \sim \sqrt{Dt} \quad \text{Equation 1}$$

238 where  $D$  is the diffusion coefficient ( $5 \times 10^{-10} \text{ cm}^2/\text{s}$  for oocysts) [6], [17]. This would  
239 suggest that oocysts diffuse around 0.002 mm in ten minutes.

240

241 However, consideration of diffusion may not be appropriate for oocysts as it  
242 has been reported that for micron-sized particles [24], hydrodynamic and gravitational  
243 forces are often significant compared to Brownian forces [18]. In the static case,  
244 hydrodynamic forces are not relevant and the gravitational force can be determined  
245 using the particle free settling velocity,  $U_s$ . This is given by:

$$246 \quad U_s = \frac{2\Delta\rho g\alpha^2}{9\mu} \quad \text{Equation 2}$$

247 where  $\Delta\rho$  ( $\text{kg}/\text{m}^3$ ) is the particle density (1045.4) minus the density of water (997),  $g$   
248 is the acceleration of gravity ( $9.81 \text{ m}/\text{s}^2$ ),  $\alpha$  is the particle radius ( $2.5 \text{ }\mu\text{m}$  for *C.*  
249 *parvum*) and  $\mu$  is the water viscosity ( $8.91 \times 10^{-4} \text{ kg}/\text{ms}$ ), and is  $0.74 \text{ }\mu\text{m}/\text{s}$  for *C.*  
250 *parvum*. Our calculated figure compares to the slightly lower values of  $0.35$  and  $0.5$   
251  $\mu\text{m}/\text{s}$  reported in the literature. Although oocyst travel by sedimentation is around an  
252 order of magnitude greater than that of diffusion, and additionally is focused in the  
253 direction of the substrate, this is still unlikely to enable efficient delivery of oocysts to  
254 the cantilever surface within ten minutes, since using an average of the above values  
255 of  $0.53 \text{ }\mu\text{m}/\text{s}$ , allows for a distance of only  $0.31 \text{ mm}$  to be covered. If a test volume of  
256  $0.1 \text{ mL}$  was utilised it would take days (assuming the volume was solely located on  
257 top of the cantilever). However, the non-flow set-up also has the disadvantage that in  
258 the flow cell set-up, which is wider, longer and deeper than the cantilever, many  
259 oocysts will initially be distributed under or to the sides of the cantilever and therefore  
260 be unable to reach the binding surface, especially allowing for sedimentation. Oocysts  
261 could not be detected even after 1 hr.

262

263           Within the microfluidic cantilever set-up, both diffusion and settling are still  
264 valid methods of oocyst transport to the surface within the channel laminar flow  
265 environment. Given the volume of the channel (0.0036  $\mu\text{L}$ ) and the flow rate (1  
266 mL/hr) it is clear that the transit time within the channel is much less than 1s. With a  
267 channel height of 20  $\mu\text{m}$  the maximal distance (in the z direction) to be travelled by  
268 an oocyst within this time is 10  $\mu\text{m}$  (allowing for the size of the oocyst). It must  
269 however be remembered that there is an even distribution of oocysts across the  
270 channel height and many will need to travel significantly less than this distance to  
271 reach the binding surface. While it is clear that not all oocysts will reach the surface  
272 even in the microfluidic cantilever set-up the chances are greatly improved. Increasing  
273 the number of encounters with the immobilised antibodies increases the likelihood of  
274 a binding event occurring and will therefore increase the capture efficiency of the  
275 system.

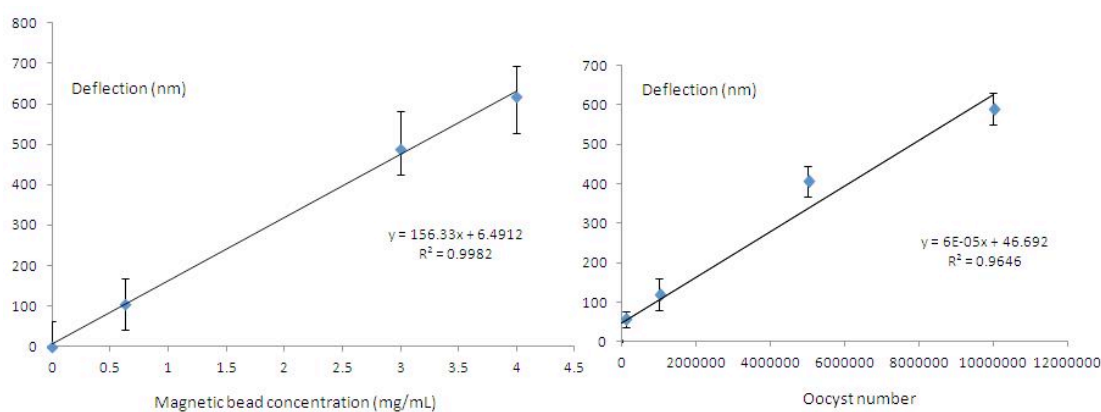
276

277           With the microfluidic cantilever system a series of different *Cryptosporidium*  
278 concentrations ( $10^5$  to  $10^7$  oocysts/mL) were investigated, with each concentration  
279 repeated five times. Following capture of the oocysts, the system was flushed with  
280 magnetic beads to amplify the signal. Figure 3B shows representative traces of the  
281 experiments, from the oocyst addition stage until the final detection point at which the  
282 unbound magnetic beads are removed from the system. One trace for each  
283 concentration is shown along with a reference sample where no *Cryptosporidium* was  
284 added. As the magnetic beads flow through the system little difference is observed  
285 between the different samples. However, upon rinsing of the magnetic beads from the  
286 system the reference sample returns to zero, whereas for the oocyst samples magnetic  
287 beads remain bound to oocysts within the system and can be utilised to determine the  
288 *Cryptosporidium* concentration in the sample. In short, Figure 3B illustrates that  
289 quantitative detection of oocysts can occur within the range  $10^5$  to  $10^7$  oocysts/mL.

290

291           The results of all five experiments have been averaged and are presented in  
292 Figure 4. The results indicate a linear relationship ( $R^2 = 0.96$ ) confirming detection in  
293 the range  $10^5$  to  $10^7$  oocysts/mL. The upper limit of  $10^7$  oocysts/mL was the highest  
294 concentration tested in this set-up and could potentially be extended. This is limited  
295 by the space for oocyst binding within the microchannel. Interestingly, a calculation

296 of the maximum coverage of the microchannel area revealed that it would be  
297 saturated with  $\sim 1 \times 10^6$  oocysts, using an oocyst diameter of  $5 \mu\text{m}$ , a channel area of  $18$   
298  $\text{mm}^2$  (assuming oocysts only bind to the immobilised antibody and not to other  
299 channel surfaces) and assuming a maximum close-packing of 74%. This calculation  
300 reveals that although the use of the microchannel improves the capture efficiency, the  
301 system still misses some oocysts. By decreasing the flow rate more time would be  
302 available for oocysts to bind within the channel, thus increasing the sensitivity. There  
303 is thus a trade-off between reaching highly sensitive detection limits and achieving a  
304 reasonable throughput/detection time, which is a recurring challenge for biosensor  
305 system for waterborne pathogens.  
306



307  
308 Figure 4. Plot of deflection (nm) against magnetic bead concentration (left graph) and oocyst number  
309 (right graph) showing a linear trends in cantilever response against magnetic bead concentration  
310 (confirming that the magnetic enhancement of detection is quantitative) and oocyst exposure.

311  
312 For practical applications, achieving a low limit of detection is the critical  
313 parameter. Lower concentrations were found not to yield a measurable response.  
314 While the sensitivity of the approach is comparable to the  $1 \times 10^5$  oocysts/mL detection  
315 limit reported for QCM-D detection of this parasite (Poitras 2009), lower  
316 concentrations have been determined, by Mutharasan and colleagues (Campbell  
317 2008), with a macrocantilever set-up. However, this operates with a recirculating flow  
318 system, which could potentially also increase the capture efficiency of the  
319 microcantilever sensor. Additionally, sensitivity could be improved by increasing the  
320 magnetic bead concentration or utilising a more powerful magnet.

321

## 322 **Conclusions**

323 The results in this paper represent the first example of a microfluidic  
324 microcantilever sensor fabricated in polyimide. Using polymer materials to  
325 manufacture the system is an advance over previous work, allowing for cheap and  
326 easy fabrication, resulting in cheap sensors which can be rapidly produced. A further  
327 advantage of this approach relates to the effective sample delivery enabled by  
328 confining the sample to a narrow layer above the cantilever surface. Transport of the  
329 analyte of interest to the capture region is often the time-limiting step and this design  
330 offers a mechanism of effective surface delivery. This is likely to prove advantageous  
331 for applications detecting rare analytes as well as in applications where very small  
332 samples are to be processed. For larger samples throughput within the microfluidic  
333 channels is potential challenge though parallelisation is an option to overcome this  
334 possible limitation. Future work could incorporate cantilever sensors on the ends of  
335 optical fibres moving towards a miniaturised portable system [19].

336

337 Furthermore, this paper has applied the system for the detection of the problematic  
338 waterborne protozoan parasite *Cryptosporidium*, demonstrating sensitivities  
339 comparable to existing literature reports and particularly showing greater sensitivity  
340 than QCM. Future work will concentrate on the optimisation of the system as well as  
341 developments in the immobilisation chemistry and the sample pre-processing to  
342 deliver even lower limit of detection, suitable for real-world application of this  
343 technology to waterborne pathogen detection.

344

345 **Acknowledgements:** HB would like to acknowledge the Royal Academy of  
346 Engineering/EPSRC for her Fellowship.

347

348

349

## 350 **References**

- 351 1. Liu, D. and W. Shu, *Microcantilever Biosensors: Probing Biomolecular*  
352 *Interactions at the Nanoscale* Current Organic Chemistry, 2011. **15**(4): p. 477-  
353 485.

- 354 2. Goeders, K.M., J.S. Colton, and L.A. Bottomley, *Microcantilevers: Sensing*  
355 *Chemical Interactions via Mechanical Motion*. Chemical Reviews, 2008. **108**:  
356 p. 522-542.
- 357 3. Takahashi, H., et al., *Differential pressure sensor using a piezoresistive*  
358 *cantilever*. Journal of Micromechanics and Microengineering, 2012. **22**: p.  
359 055015.
- 360 4. Rasmussen, P.A., A.V. Grigorov, and A. Boisen, *Double sided surface stress*  
361 *cantilever sensor*. Journal of Micromechanics and Microengineering, 2005.  
362 **15**: p. 1088.
- 363 5. Burg, T.P., et al., *Weighing of biomolecules, single cells and single*  
364 *nanoparticles in fluid*. Nature, 2007. **446**(7139): p. 1066-1069.
- 365 6. Squires, T.M., R.J. Messinger, and S.R. Manalis, *Making it stick: convection,*  
366 *reaction and diffusion in surface-based biosensors*. Nat Biotechnol, 2008.  
367 **26**(4): p. 417-426.
- 368 7. Liju, Y., *Dielectrophoresis assisted immuno-capture and detection of*  
369 *foodborne pathogenic bacteria in biochips*. Talanta, 2009. **80**(2): p. 551-558.
- 370 8. Johansson, A., et al., *SU-8 cantilever sensor system with integrated readout*.  
371 *Sensors and Actuators A: Physical*, 2005. **123**: p. 111-115.
- 372 9. Calleja, M., et al., *Polymeric mechanical sensors with piezoresistive readout*  
373 *integrated in a microfluidic system in Microtechnologies for the New*  
374 *Millennium 2003*. 2003: 7th International Conference on Miniaturized  
375 Chemical and Biochemical Analysts Systems
- 376 10. Ricciardi, C., et al., *Integration of microfluidic and cantilever technology for*  
377 *biosensing application in liquid environment*. Biosensors and Bioelectronics,  
378 2010. **26**(4): p. 1565-1570.
- 379 11. Okhuysen, P.C., et al., *Virulence of three distinct Cryptosporidium parvum*  
380 *isolates for healthy adults*. Infectious Diseases, 1999. **180**: p. 1275-1281.
- 381 12. King, B.J. and P.T. Monis, *Critical processes affecting Cryptosporidium*  
382 *oocyst survival in the environment*. Parasitology, 2007. **134**: p. 309-323.
- 383 13. Bridle, H., et al., *Detection of Cryptosporidium in miniaturised fluidic devices*.  
384 *Water Research*, 2012. **46**(6): p. 1641-1661.
- 385 14. Poitras, C., J. Fatisson, and N. Tufenkji, *Real-time microgravimetric*  
386 *quantification of Cryptosporidium parvum in the presence of potential*  
387 *interferents*. Water Research, 2009. **43**(10): p. 2631-2638.
- 388 15. Campbell, G.A. and R. Mutharasan, *Near real-time detection of*  
389 *Cryptosporidium parvum oocyst by IgM-functionalized piezoelectric-excited*  
390 *millimeter-sized cantilever biosensor*. Biosensors and Bioelectronics, 2008.  
391 **23**(7): p. 1039-1045.
- 392 16. Gavriilidou, D. and H. Bridle, *Comparison of immobilisation strategies for*  
393 *Cryptosporidium parvum immunosensors*. Biochemical Engineering Journal,  
394 2012. **68**: p. 231-235.
- 395 17. Gervaise, P. and P. Molin, *The role of water in solid-state fermentation*.  
396 *Biochemical Engineering Journal*, 2003. **13**: p. 85-101.
- 397 18. Yiantsios, S.G. and A.J. Karabelas, *Deposition of micron-sized particles on*  
398 *flat surfaces: effects of hydrodynamic and physicochemical conditions on*  
399 *particle attachment efficiency*. Chemical Engineering Science, 2003. **58**(14):  
400 p. 3105-3113.
- 401 19. Albri, F., et al., *Laser machining of sensing components on the end of optical*  
402 *fibres*. Journal of Micromechanics and Microengineering, 2012. **23**(4): p.  
403 045021.

